GEOPHYSICS, VOL. 78, NO. 2 (MARCH-APRIL 2013); P. WA77–WA89, 12 FIGS., 3 TABLES.
10.1190/GEO2012-0295.1

First application of Green's theorem-derived source and receiver deghosting on deep-water Gulf of Mexico synthetic (SEAM) and field data

James D. Mayhan[1] and Arthur B. Weglein[1]

ABSTRACT

Deghosting benefits traditional seismic processing and is a prerequisite to all inverse-scattering-series based processing. The freedom of choosing a convenient reference medium (and associated Green's function) means Green's theorem offers a flexible framework for deriving useful algorithms including deghosting. Among advantages over traditional deghosting methods are: (1) no need for Fourier transforms over receivers and sources, and (2) can accommodate a horizontal or non-horizontal measurement surface, the latter of particular interest for ocean bottom and onshore applications. The theory of Green's theorem-derived deghosting is presented, and its first application on deep-water Gulf of Mexico synthetic (SEAM) and field data is reported. The source and receiver deghosting algorithms work with positive and encouraging results.

INTRODUCTION

Deghosting is a long-standing problem (see, e.g., Robinson and Treitel, 2008) and benefits traditional seismic processing and all inverse-scattering-series (ISS) based processing. The benefits of deghosting include the following: (1) removing the downward component of the recorded pressure wavefield (receiver deghosting) enhances seismic resolution by removing ghost notches and boosting low frequencies, (2) deghosting is a prerequisite for many processing algorithms including multiple elimination (ISS free-surface multiples, ISS internal multiples, and surface-related-multiple elimination), and (3) model-matching full-wave inversion (FWI) benefits from enhanced low-frequency data.

Although ISS methods are independent of subsurface velocity (and in fact of all subsurface properties), they make certain assumptions about their input data. Weglein et al. (2003) describe how every ISS isolated-task subseries requires (1) the removal of the reference wavefield, (2) an estimate of the source signature and radiation pattern, and (3) source and receiver deghosting, and how the ISS has a nonlinear dependence on these preprocessing steps. The fact that the ISS is nonlinear places a higher premium on preprocessing requirements. An error in the input to a linear process creates a linear error in its output, but the same linear error in ISS input creates a combination of linear, quadratic, cubic, etc., errors in its output. The non-linear model matching FWI would share that interest.

The freedom of choosing a convenient reference medium (and associated Green's function) means Green's theorem offers a flexible framework for deriving useful algorithms. Green's theorem methods can be categorized as wavefield prediction or wavefield separation. To predict the wavefield anywhere in a volume V, Green's theorem based wavefield prediction has the traditional need for (a) wavefield measurements on the boundary S enclosing V and (b) a knowledge of the medium throughout V. Examples of wavefield prediction based on Green's theorem include Schneider (1978), Clayton and Stolt (1981), Stolt and Weglein (2012), and reverse-time migration (Weglein et al., 2011a, 2011b). In contrast, Green's theorem-based wavefield separation only assumes separate sources inside and outside V, and nothing about the character of those sources is called for or needed. Within wavefield separation, different applications (e.g., wavelet estimation and deghosting) call for different choices of reference media and sources. Examples of wavefield separation based on Green's theorem include source-wavelet estimation (Weglein and Secrest, 1990) and deghosting (Weglein et al., 2002; Zhang and Weglein, 2005, 2006; Zhang, 2007). In Green's theorem wavefield separation methods, evaluating the surface integral at a point inside V provides the contribution to the total field at a point inside V due to sources outside V, without needing or determining the nature or properties of any of the actual (active or passive) sources inside or outside V. Hence, Green's theorem-derived wavefield separation preprocessing steps (e.g., for wavelet

Manuscript received by the Editor 28 July 2012; revised manuscript received 18 December 2012; published online 20 March 2013.
[1]University of Houston, M-OSRP, Houston, Texas, USA. E-mail: jdmayhan@uh.edu; aweglein@uh.edu.

estimation and deghosting) are consistent with subsequent ISS processing methods that also do not assume knowledge of or require subsurface information. The Green's theorem wavefield prediction and wavefield separation methods are multidimensional and work in the $(\mathbf{r}, \omega)$ or $(\mathbf{r}, t)$ data spaces (and, hence, are simple to apply to irregularly spaced data).

Green's theorem-derived deghosting was developed in a series of papers (Weglein et al., 2002; Zhang and Weglein, 2005, 2006; Zhang, 2007) and has characteristics not shared by previous methods. For example, there is no need for Fourier transforms over receivers and sources, and it can accommodate a horizontal or non-horizontal measurement surface. In Mayhan et al. (2011), we reported the first use of Green's theorem-derived receiver deghosting on deep-water Gulf of Mexico synthetic (SEAM) and field data; in Mayhan et al. (2012), we reported the first use of Green's theorem-derived source deghosting on the same data; and in this paper we provide more detail on the algorithms used.

A brief aside on our terminology. (1) The total wavefield P measured by the hydrophones is considered as the sum of a reference wavefield P_0 (which for a homogeneous whole-space reference medium (used in Green's theorem deghosting) is a direct wave from source to receiver) and the scattered wavefield P_s (which is $P - P_0$). (2) Ghosts begin their propagation moving upward from the source (source ghosts) or end their propagation moving downward to the receiver (receiver ghosts) or both (source/receiver ghosts) and have at least one upward reflection from the earth.

After the reference wavefield and all ghosts have been removed, multiples and primaries are defined. (3) Free-surface multiples have at least one downward reflection from the air/water boundary and more than one upward reflection from the earth. (An nth order free-surface multiple has n downward reflections from the air/water boundary.) (4) Internal multiples have no downward reflections from the air/water boundary, more than one upward reflection from the earth, and at least one downward reflection from below the free surface. (An nth order internal multiple has n downward reflections from any reflector(s) below the free surface.) (5) Primaries have only one upward reflection from the earth. These marine events are summarized in Figure 1.

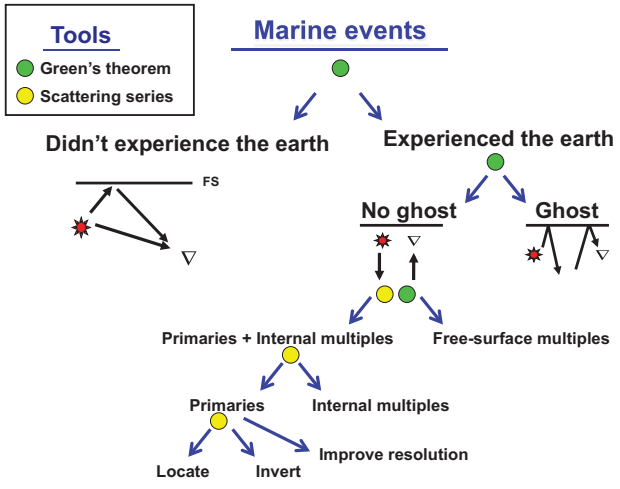

Figure 1. Classification of marine events and how they are processed.

The source- and receiver-deghosting steps described below essentially follow the method described and exemplified in pages 33–39 of Zhang (2007). The difference is that for each shot we choose to input dual measurements of P and $\partial P/\partial z$ along the towed streamer, whereas Zhang chose to use the source wavelet and P along the cable for his numerical examples. (The theory in Zhang [2007] covers both cases.) The advantages of having the wavefield P and its normal derivative along the towed streamer are (1) to allow deghosting for an arbitrary source distribution without needing to know or to determine the source, and (2) for increased stability in the vicinity of notches. Using measurements at two depths (or G_0^{DD} as described below) introduces a more depth-sensitive denominator.

THEORY

Receiver deghosting

Green's theorem derived-preprocessing is based on a perturbation approach where the actual problem and medium are considered as composed of a reference medium plus "sources." The latter arise as source terms in the differential equation that describes the wave propagation in the actual medium. A reference medium (and its associated Green's function) is chosen to facilitate solving the problem at hand, and the perturbations are represented as source terms necessary to write the actual propagation in terms of a reference medium source term picture. Within that general reference medium and source term framework, Green's theorem-derived preprocessing is remarkably wide ranging. For example, Figure 2 shows the configuration chosen for Green's theorem-derived deghosting. For deghosting, a reference medium that consists of a whole-space of water requires three source terms: a source that corresponds to air and begins above the air-water boundary, the air guns in the water column, and a source that corresponds to earth and begins below the water-earth boundary. Choosing a hemispherical surface of integration bounded below by the measurement surface, and the prediction or observation point inside the surface of integration

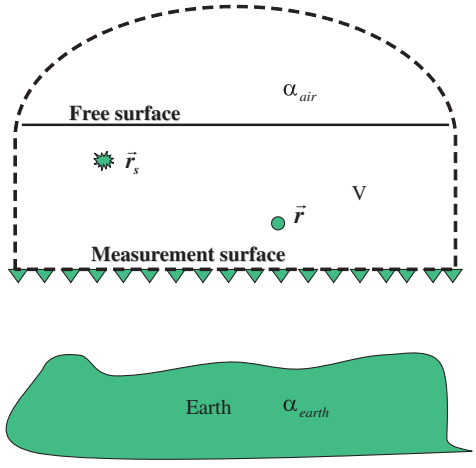

Figure 2. Configuration for Green's theorem-derived deghosting (Zhang [2007] Figure 2.10). α_{air} and α_{earth} are perturbations, the differences between the actual medium (half-space of air, water, half-space of earth) and the reference medium (whole-space of water). The closed surface S of integration is the measurement surface plus the dashed line. $\mathbf{r}$ in the figure corresponds to $\mathbf{r}_g'$ in equation 2.

gives receiver-deghosted data, P'_R (as explained in Appendix A). A different choice of a reference medium (a half-space of air and a half-space of water, separated by an air/water boundary) with two source terms, is useful for separating the reference wave P_0=$P_0^d + P_0^{FS}$ and $P_s = P - P_0$. The prediction or observation point outside or inside the surface of integration, gives wavefield separation, in which the total wavefield P is separated into the reference wavefield P_0 (prediction or observation point outside) or the scattered wavefield P_s (prediction or observation point inside).

Green's theorem-derived deghosting (receiver and source) is based on Weglein et al. (2002), Zhang and Weglein (2005, 2006), and Zhang (2007). Depending on the marine experiment, we have the following options for receiver deghosting. (1) If we have P measurements only, we can use a derived variation of Green's theorem (equation 3), a "double Dirichlet" Green's function (equation 7 or 8), and an estimate of the source wavelet to predict P and $\partial P/\partial z$ above the towed streamer(s). Then we can use the derived variation of Green's theorem, a "whole-space" Green's function (equation 1), and the predicted P and $\partial P/\partial z$ to predict receiver-deghosted P'_R above the input P and $\partial P/\partial z$. (2) If we have a dual-sensor towed streamer or over/under towed streamers, we can use the derived variation of Green's theorem and a whole-space Green's function to directly predict receiver-deghosted P'_R above the towed streamer(s). The theory of case (2) assumes measurement of the pressure wavefield P and its normal derivative $\partial P/\partial n \equiv \nabla P(\mathbf{r}, \mathbf{r}_s, \omega) \cdot \hat{\mathbf{n}}$ where $\mathbf{r}$ is the receiver location, $\mathbf{r}_s$ is the source location, and $\hat{\mathbf{n}}$ is the unit normal to the measurement surface (pointing away from the enclosed volume V).

The reference medium is chosen to be a whole-space of water (where a causal solution exists for the acoustic wave equation in 3D). In the $(\mathbf{r}, \omega)$ domain, the causal whole-space Green's function is

$$G_0(\mathbf{r}, \mathbf{r}'_g, \omega) = G_0^d = \begin{cases} -(1/4\pi)\exp(ikR_+)/R_+ & \text{in 3D} \\ -(i/4)H_0^{(1)}(kR_+) & \text{in 2D} \end{cases} \tag{1}$$

where $\mathbf{r}'_g$ is the observation or prediction location, $k = \omega/c_0$, c_0 is the wave speed in the reference medium, $R_+ = |\mathbf{r} - \mathbf{r}'_g|$, and $H_0^{(1)}$ is the zeroth-order Hankel function of the first kind (Morse and Feshbach [1953], § 7.2). The observation or prediction point is chosen between the air/water boundary and the measurement surface, i.e., inside the volume V bounded by the closed surface of integration consisting of the measurement surface and the dashed line in Figure 2. For a discussion of why the causal whole-space Green's function exhibits the forms in equation 1, please see chapter 7 in Morse and Feshbach (1953).

The configuration in Figure 2, the derived variation of Green's theorem, and the acoustic wave equations for P and G_0^d combine to give the key equation,

$$P'_R(\mathbf{r}'_g, \mathbf{r}_s, \omega) = \oint_S dS\, \hat{\mathbf{n}} \cdot [P(\mathbf{r}, \mathbf{r}_s, \omega)\nabla G_0^d(\mathbf{r}, \mathbf{r}'_g, \omega) - G_0^d(\mathbf{r}, \mathbf{r}'_g, \omega)\nabla P(\mathbf{r}, \mathbf{r}_s, \omega)], \tag{2}$$

where S is the closed surface consisting of the measurement surface and the dashed line in Figure 2, and $\hat{\mathbf{n}}$ is the unit normal to S (pointing away from the enclosed volume V). The source location, $\mathbf{r}_s$, and observation or prediction point, $\mathbf{r}'_g$, are inside the volume V. Extending the radius of the hemisphere to infinity, invoking the Sommerfeld radiation condition, and assuming a horizontal measurement surface, the integral over the closed surface becomes an integral over the measurement surface (Weglein et al. [2002] equation 5),

$$P'_R(\mathbf{r}'_g, \mathbf{r}_s, \omega) = \int_{m.s.} dS \left[P(\mathbf{r}, \mathbf{r}_s, \omega) \frac{\partial}{\partial z} G_0^d(\mathbf{r}, \mathbf{r}'_g, \omega) - G_0^d(\mathbf{r}, \mathbf{r}'_g, \omega) \frac{\partial}{\partial z} P(\mathbf{r}, \mathbf{r}_s, \omega) \right]. \tag{3}$$

The algorithm in equation 3 lends itself to application in a marine single-shot experiment. If the predicted cable is above the towed cable and below the shots, equation 3 identifies and attenuates downgoing waves at the predicted cable (as shown in Appendix A). Receiver ghosts, source/receiver ghosts, the direct wave, and the direct wave's reflection at the air/water boundary are removed.

Green's theorem derived receiver deghosting can be compared with a conventional $P + V_z$ sum method of deghosting (Amundsen, 1993; Robertsson and Kragh, 2002; Kragh et al., 2004). For a 3D point source and given a 1D earth and horizontal acquisition and adequate sampling to allow a Fourier transform from space to wavenumber, the two algorithms are equivalent. But these givens can be an issue. In addition, the application of the $P + V_z$ sum, under certain circumstances, brings other assumptions. For example, a 1D layered earth is assumed and dense sampling is needed to support its inverse Hankel transform (Amundsen [1993], p. 1336). The latter is often considered the current industry standard deghosting method. In contrast, the Green's theorem deghosting algorithm (1) can accommodate a 1D, 2D, or 3D earth and (2) stays in coordinate space. Within these assumptions, $P + V_z$ can be derived from Green's theorem as shown in Appendix B. The derivation follows in the tradition of Corrigan et al. (1991), Amundsen (1993), Weglein and Amundsen (2003); Weglein et al. (personal communication, 2013). This derivation, which to our knowledge has not been

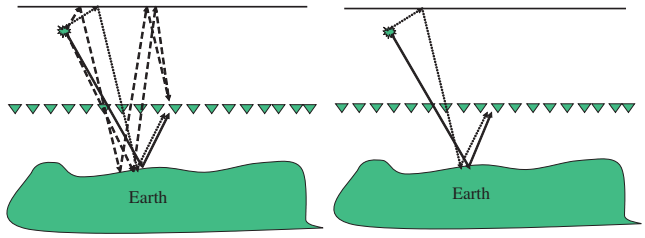

Figure 3. Input (left), receiver deghosted (right) (Zhang [2007] Figure 2.14).

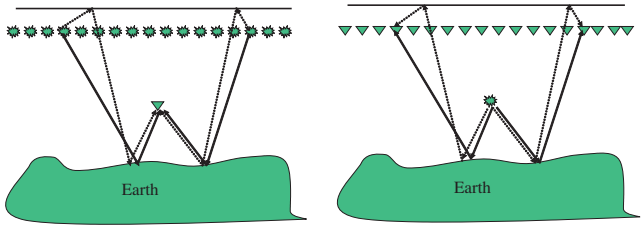

Figure 4. CSG to CRG (left), exchange coordinates (right) (Zhang [2007] Figure 2.15–2.16).

published before, shows that deghosting in the wavenumber-frequency domain is a special case of the more general deghosting in the space-frequency domain derived from Green's theorem.

Source deghosting

We have shown how Green's theorem can be applied to select the portion of the seismic wavefield that is upgoing at a field position above the cable. The algorithm uses data from a single shot gather and the receiver coordinate as the integration variable. This section shows how the theory can be similarly applied for source deghosting, where the portion of the wavefield that is downgoing at the source is sought. Depending on the marine experiment, we have the following options for source deghosting. (1) If we have a collection of single source experiments, we can use the derived variation of Green's theorem (equation 3), a double Dirichlet Green's function (equation 7 or 8), and receiver-deghosted data P'_R to predict new P'_R and $\partial P'_R/\partial z$ above the receiver-deghosted data. Then we can use the derived variation of Green's theorem, a whole-space Green's function (equation 1), and the predicted P'_R and $\partial P'_R/\partial z$ to predict source and receiver-deghosted P'_{SR} above the input P'_R and $\partial P'_R/\partial z$. (2) If we have over/under shots, we can use the derived variation of Green's theorem (equation 4), a whole-space Green's function, and receiver-deghosted data P'_R to directly predict source and receiver-deghosted P'_{SR} above the receiver-deghosted data. An application of reciprocity to the entire set of shot records allows the original receiver-ghost removal to become a source-ghost removal. Then a second application of the derived variation of Green's theorem over receivers results in source- and receiver-deghosted data. An experiment with over/under receivers and over/under sources can be receiver deghosted and source deghosted by a double application of the derived variation of Green's theorem (part of Weglein et al., 2002).

Green's theorem-derived source deghosting begins with source-receiver reciprocity. We interpolate shots so that the distance between shots is the same as the inline distance between receivers, assign "station numbers" to shots and receivers relative to a grid fixed in space, use the station numbers to re-sort the sail line from common-shot gathers (CSGs) to common-receiver gathers (CRGs), and exchange the locations of the shots and receivers. Source ghosts upgoing at the shots are now receiver ghosts downgoing at the "receivers," and a second application of equation 3 will remove them. This can be seen in Figures 3 and 4. In Figure 3, the left panel shows the recorded data (for simplicity, only primaries and their ghosts are shown), and the right panel shows receiver-deghosted data (the receiver ghosts and source/receiver ghosts have been attenuated leaving primaries and their source ghosts). In the left panel of Figure 4, CSGs have been sorted to produce CRGs, and in the right panel shot and receiver locations have been exchanged. The configuration in panel (d) looks like that in panel (a), so a second application of equation 3 will remove the source ghosts.

If the experiment has over/under shots, the integral analogous to equation 3 is

$$P'_{SR}(\mathbf{r}'_g,\mathbf{r}'_s,\omega)=\int_{\text{sources}} dS\,\hat{\mathbf{n}}\cdot[P'_R(\mathbf{r}'_g,\mathbf{r},\omega)\nabla G_0^+(\mathbf{r},\mathbf{r}'_s,\omega) - G_0^+(\mathbf{r},\mathbf{r}'_s,\omega)\nabla P'_R(\mathbf{r}'_g,\mathbf{r},\omega)]. \quad (4)$$

With single shot experiments, the next step in Green's theorem-derived source deghosting predicts a dual-sensor cable. Now (following Zhang (2007)) use a double Dirichlet Green's function G_0^{DD} to predict a dual-sensor cable above the receiver-deghosted cable. G_0^{DD} is constructed to vanish on the air/water boundary and the measurement surface (Morse and Feshbach [1953], p. 812ff; Osen et al., 1998; Tan, 1999; Zhang [2007], p. 20ff). In the $(\mathbf{r},\omega)$ domain, Green's theorem now takes the form

$$P'_R(\mathbf{r}''_g,\mathbf{r}_s,\omega)=\int_{m.s.} dS'_g P'_R(\mathbf{r}'_g,\mathbf{r}_s,\omega)\frac{\partial G_0^{DD}}{\partial z_g{}'}(\mathbf{r}'_g,\mathbf{r}''_g,\omega)|_{z'_g=m.s.} \quad (5)$$

$$\frac{\partial P'_R}{\partial z''_g}(\mathbf{r}''_g,\mathbf{r}_s,\omega)=\int_{m.s.} dS'_g P'_R(\mathbf{r}'_g,\mathbf{r}_s,\omega)\frac{\partial^2 G_0^{DD}}{\partial z'_g\partial z''_g}(\mathbf{r}'_g,\mathbf{r}''_g,\omega)|_{z'_g=m.s.} \quad (6)$$

where $\mathbf{r}''_g$ is the observation or prediction point, $\mathbf{r}_s$ is the shot location, $\mathbf{r}'_g$ is the receiver location on the receiver-deghosted cable, and

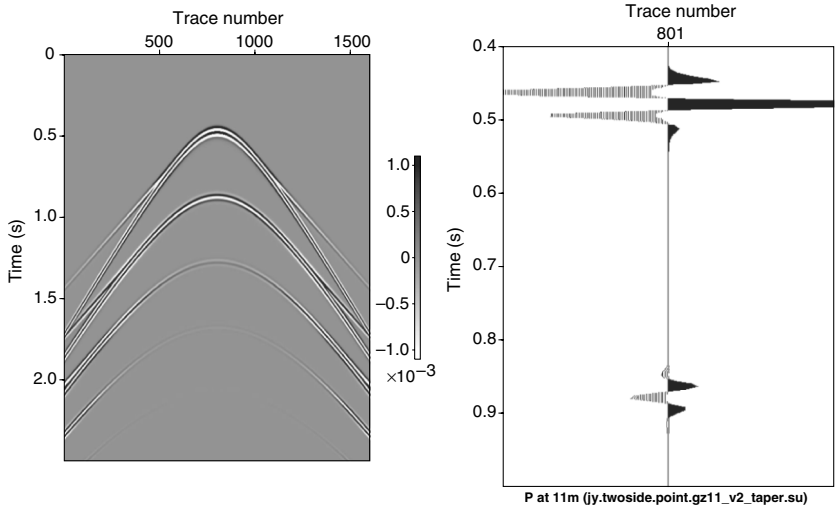

Figure 5. Flat-layer model: P_s at 11 m. The first event is the water bottom primary and its ghosts, and the second event is the first free surface multiple and its ghosts. The right panel shows the zero-offset trace (801 of 1601). More detail is given in Table C-1 in Appendix C.

differentiating equation 5 with respect to the observation or prediction coordinate z_g'' derives equation 6. P_R' is the result of receiver deghosting and source-receiver reciprocity. For a single source experiment, source and receiver deghosting is achieved (with over/under receivers) first using equation 3 and then substituting equations 5 and 6 in equation 4.

In 2D the analytic form of the double Dirichlet Green's function G_0^{DD} in the $(\mathbf{r}, \omega)$ domain is

$$G_0^{DD}(\mathbf{r}_g', \mathbf{r}_g'', \omega) = -\frac{1}{b}\sum_{n=1}^{\infty}\frac{1}{\sqrt{\beta}}\exp\left(-\sqrt{\beta}|x_g' - x_g''|\right) \times \sin\left(\frac{n\pi}{b}z_g'\right)\sin\left(\frac{n\pi}{b}z_g''\right) \quad (7)$$

where (x_g'', z_g'') are the observation or prediction coordinates, (x_g', z_g') are the receiver coordinates on the receiver-deghosted cable, the air/water boundary is at $z_g' = 0$, the input (receiver-deghosted) cable is at $z_g' = b$, and we assume $\beta \equiv (n\pi/b)^2 - k^2 > 0$ (Osen et al., 1998; Tan, 1999). In 3D,

$$G_0^{DD}(\mathbf{r}_g'', \mathbf{r}_g', \omega) = \frac{2\pi i}{b}\sum_{n=1}^{\infty}H_0^{(1)}(\gamma\rho)\sin\left(\frac{n\pi}{b}z_g'\right)\sin\left(\frac{n\pi}{b}z_g''\right) \quad (8)$$

where $\gamma = i\sqrt{\beta}$ and $\rho = \sqrt{(x_g'' - x_g')^2 + (y_g'' - y_g')^2}$ (Osen et al., 1998). For a discussion as to why G_0^{DD} has these forms, please see p. 820 in Morse and Feshbach (1953). For purposes of numeric evaluation, the Hankel function with imaginary argument is replaced by a hyperbolic Bessel function with real argument (Morse and Feshbach [1953], p. 1323).

The following simple analysis shows that for separating up and down waves using two measurements at one depth can be more stable than two measurements at two different depths. Using P measured at two depths introduces a depth sensitive denominator. Under perfect conditions the two methods are equivalent, but under practical conditions they are not. For example,

$$P = A\ \exp(ikz) + B\ \exp(-ikz) \quad (9)$$

$$P(0) = A + B \quad (10)$$

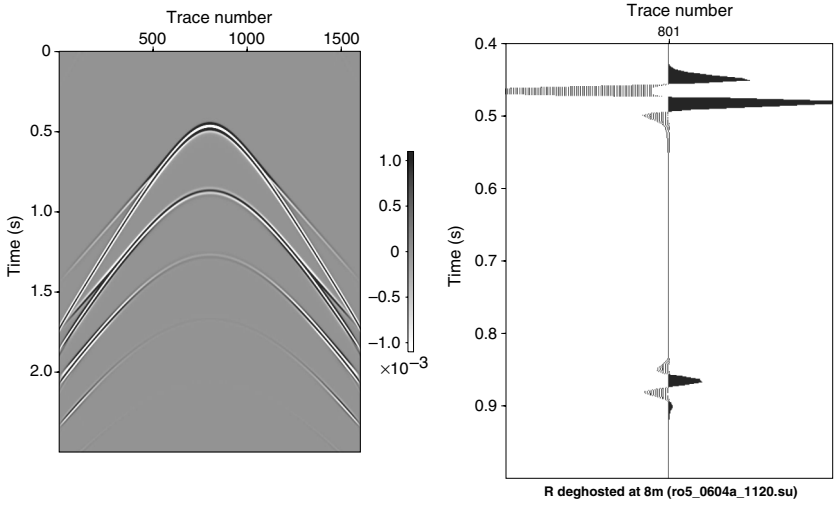

Figure 6. Flat-layer model: Receiver deghosted P_s at 8 m. Note that the receiver and source-receiver ghosts have been attenuated. The right panel shows the zero-offset trace (801 of 1601).

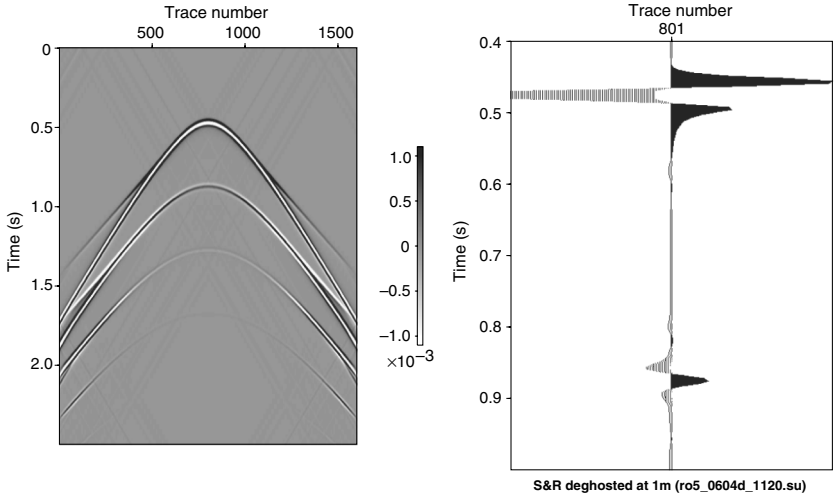

Figure 7. Flat-layer model: Source and receiver deghosted P_s at 1 m. Note that the source ghosts have been attenuated. The right panel shows the zero-offset trace (801 of 1601).

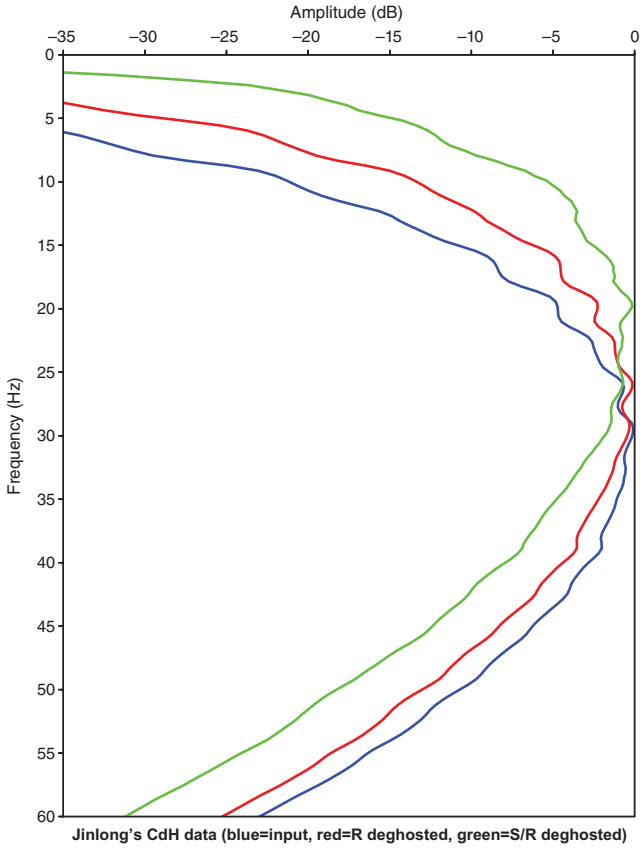

Figure 8. Flat-layer model data, spectrum of the zero-offset trace (801 of 1601): blue = input, red = receiver deghosted, green = source and receiver deghosted. Note the shift of the spectrum toward lower frequencies. Also note that source and receiver deghosting (green) has a larger effect that receiver deghosting (red). Receiver deghosting results from one application of the algorithm to measured data, whereas source and receiver deghosting results from three applications: receiver deghosting, wavefield prediction (of the receiver deghosted data at a point above the cable), and source deghosting.

$$\frac{dP}{dz}(0) = ik(A - B) \tag{11}$$

$$A = \frac{dP/dz(0) + ikP(0)}{2ik} \tag{12}$$

$$B = \frac{dP/dz(0) - ikP(0)}{-2ik} \tag{13}$$

is stable. However, measurements at two depths or G_0^{DD} (the latter comes from $G_0 = 0$ at two depths) gives

$$P(0) = A + B \tag{14}$$

$$P(a) = A\ \exp\ (ika) + B\ \exp(-ika) \tag{15}$$

$$A = \frac{P(0)\exp(-ika) - P(a)}{-2i\ \sin(ka)} \tag{16}$$

$$B = \frac{P(0)\exp(ika) - P(a)}{2i\ \sin(ka)} \tag{17}$$

which is sensitive in the vicinity of ghost notches (where $ka = n\pi$). If our interest is away from ghost notches, one-source experiments will be fine for source and receiver deghosting, whereas if our interest includes the ghost notches, two-source experiments can provide more stability for source-side deghosting. The appropriate method depends on bandwidth and depth of sources and receivers. If our sources and receivers are at the ocean bottom, ghost notches come up early and double sources would be indicated. This also impacts receiver deghosting using measurements at two depths because of sensitivity to ghost notches. The alternative method of receiver deghosting using the source wavelet $A(\omega)$, P along the cable, and the double Dirichlet Green's function G_0^{DD} allows receiver deghosting without the need for measurements at two depths, but G_0^{DD} uses information at two different depths and hence

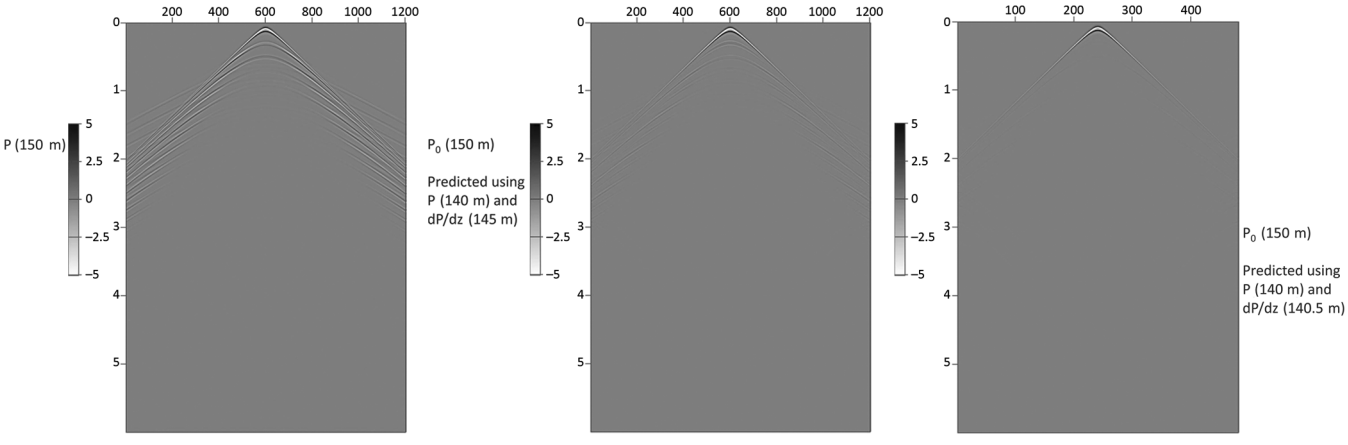

Figure 9. P at 150 m (left panel), P_0 at 150 m using 10 m between over/under cables (middle panel), P_0 at 150 m using 1 m between over/under cables (right panel). Note the "leakage" of P_s in the middle panel and the absence of visible "leakage" of P_s in the right panel.

may have stability issues compared to two measurements at one depth.

Code

The implementation of the above theory is done in a straightforward manner. The Green's theorem-derived algorithm computes the surface integral in equation 3. The method requires as input two wave fields, the pressure measurements P and their normal derivatives $\partial P/\partial z$. Measuring the latter requires a dual-sensor cable or over/under cables. The programs use data in the Seismic Unix (SU) format and integrate with all native SU programs.

RESULTS

Example: Flat-layer model

Figure 5 shows synthetic data produced using Cagniard-de Hoop code and a flat-layer model. (More detail on the input data is given in Tables C-1, C-2, and C-3 in Appendix C.) The first event is the

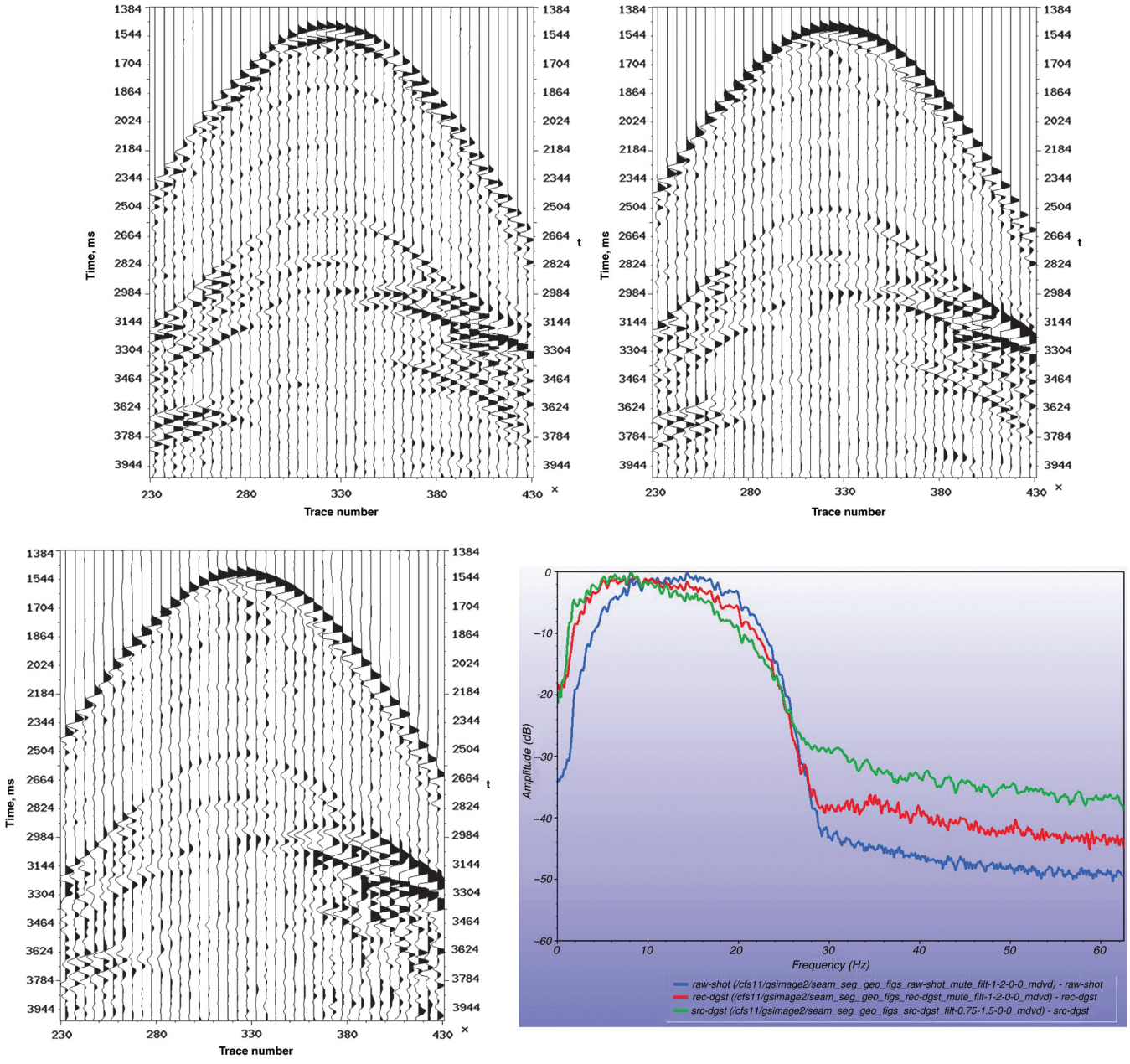

Figure 10. SEAM data, shot 131,373: recorded data at 17 m (top left), receiver deghosted at 10 m (top right), source and receiver deghosted at 10 m (bottom left). Note the collapsed wavelets in the top right and bottom left panels. Frequency spectra (bottom right): red = P at 17 m, blue = receiver deghosted at 10 m, green = source and receiver deghosted at 10 m. The spectrum uses a window of 201 traces (232–432) by 0.6 s (1.4–2.0). The first source notch is at 44 Hz which lies above the source frequency range (1–30 Hz). Note the shift of the spectrum toward lower frequencies (which may be of interest to FWI).

water-bottom primary and its source ghost, receiver ghost, and source/receiver ghost, and the second event is the first free-surface multiple and its three ghosts. Figure 6 shows Green's theorem-derived output computed using equation 3. Comparing Figures 5 and 6 shows that the receiver ghost and source/receiver ghost associated with the primary and first free-surface multiple have been attenuated. Figure 7 shows the result of source deghosting. Comparing Figures 6 and 7 shows that the source ghost has been attenuated for the first event (the water-bottom primary) and the second event (the first free-surface multiple). Deghosting also boosts low frequencies as seen in Figure 8.

Does the quality of deghosting depend on the distance between the over/under cables? Tang (L. Tang, 2013, personal communication) has used the same algorithm and a similar flat-layer model to study how a particular wavefield separation (into the reference and scattered fields) depends on this (and other) parameters. She concluded, "The estimated results get better when the over/under cables are closer to each other, i.e., P and dP/dz are approximately located at the same depth." Her results are shown in Figure 9. Robertsson and Kragh (2002) report the same result, where their upper "cable" is the air/water boundary. It is expected that the quality of deghosting is also a function of the distance between the over/under cables.

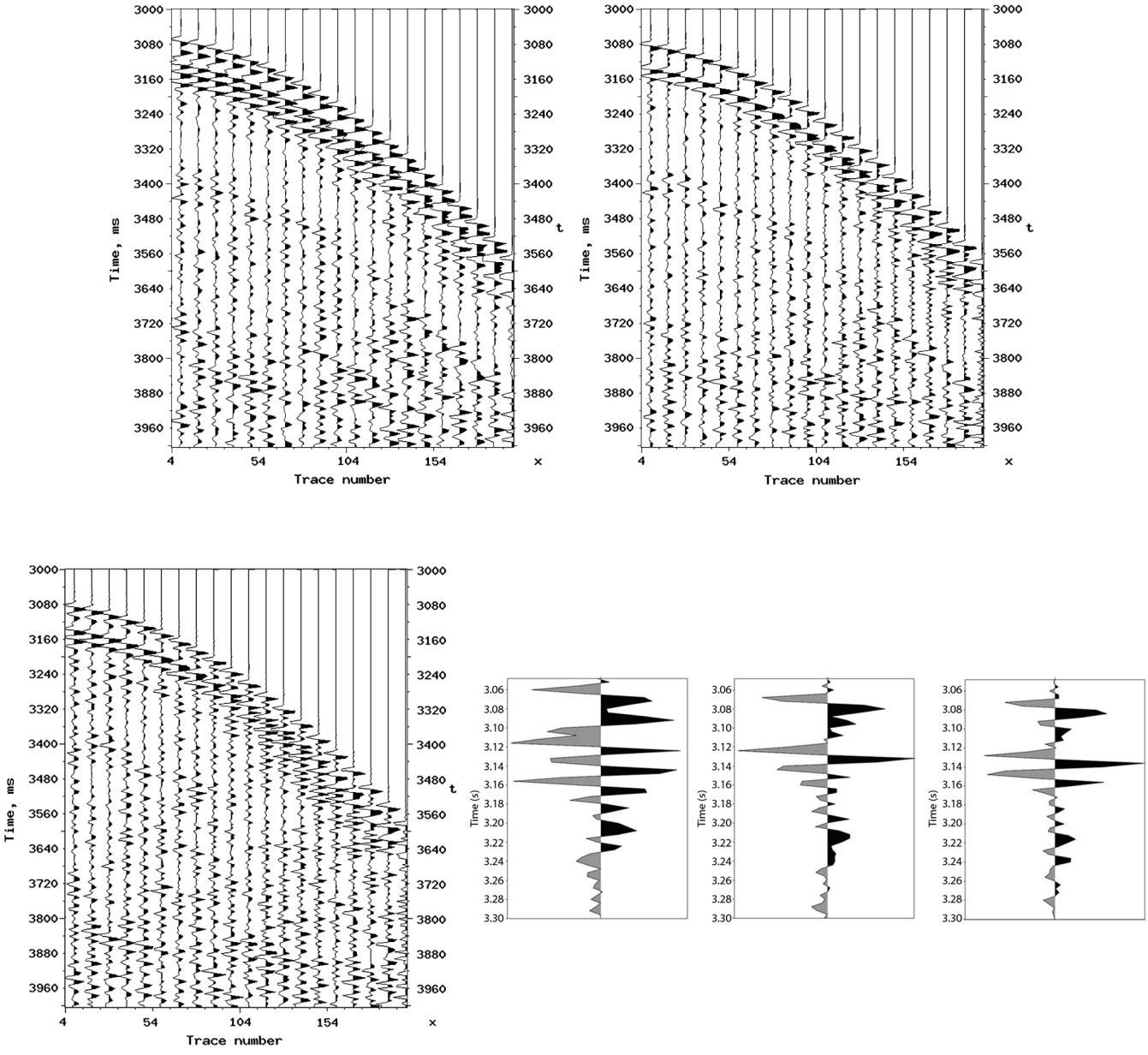

Figure 11. Field data: hydrophones at 22–25 m (top left), receiver deghosted at 10.5 m (top right), source and receiver deghosted at 8 m (bottom left). Note the collapsed wavelets in the top right and bottom left panels. Closeup of trace 5 in each of the above panels (bottom right). Note the gradual recovery of the shape of the wavelet: by receiver deghosting (middle trace) then by source and receiver deghosting (right trace). Input data courtesy of PGS.

Example: SEAM

Green's theorem-derived deghosting was applied to the SEAM data set generated based on a deep-water Gulf of Mexico earth model (SEG Advanced Modeling Corporation [SEAM], 2011). We used the special SEAM classic data set modeled to simulate dual-sensor acquisition by recording the pressure wavefield at two different depths, 15 and 17 m, respectively. This dual-sensor data consisted of nine sail lines for an equivalent wide-azimuth towed-streamer survey. The source interval is 150 × 150 m, whereas the receiver interval is 30 m in inline and crossline directions. (More detail about this data is given in Table C-2 in Appendix C.) Given the low frequency of the data (less than 30 Hz) and the source and receiver depths of 15 and 17 m, the ghost reflections are not as separable as in the previous flat layer model with deeper sources and receivers. In this shallower source and receiver situation, successful deghosting would correspond to a change in the wavelet shape. The top left panel of Figure 10 shows SEAM input, the top right panel shows receiver-deghosted output computed by the Green's theorem approach, and the bottom left panel shows source and receiver-deghosted output also computed by the Green's theorem approach. In the top right and bottom left panels of Figure 10, note the collapsed wavelet. In the bottom right panel of Figure 10, note the shift of the amplitude spectrum toward low frequencies. Deghosting reduces amplitude between notches, where constructive interference occurs between waves propagating upward and waves propagating downward. In this data, notches occur at $f = nc_0/(2z)$, i.e., at multiples of 50 Hz. Because the source energy is in frequencies less than 30 Hz, deghosting is manifested by the frequency shift.

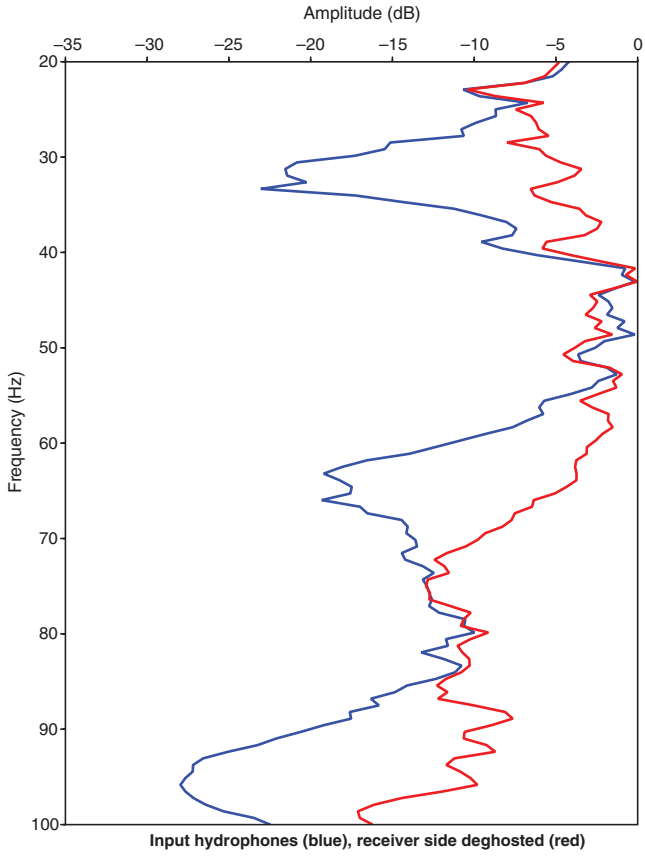

Figure 12. Field data: muted hydrophones (blue), receiver deghosted (red). The receiver notches around 30, 60, and 90 Hz have been filled in. Input data courtesy of PGS.

Example: Field data

Green's theorem-derived deghosting was also applied to a field survey from the deep-water Gulf of Mexico. The data were acquired using dual-sensor streamers comprised of hydrophones and vertical geophones. (More detail about this data is given in Table C-3 in Appendix C.) The vertical geophones measure V_z, whereas Green's theorem-derived algorithms require dP/dz. It can be shown (from the equation of motion for a fluid, see Appendix D) that the required conversion is $dP/dz = i\omega\rho V_z$, where ρ is the density of the reference medium (sea water). The top left panel in Figure 11 shows a close up of an input shot record whereas the top right panel displays the same traces after receiver deghosting and the bottom left panel displays the same traces after source and receiver deghosting. Note the collapsed wavelet in the output images. This is also demonstrated in Figure 12, which compares the amplitude spectra before and after receiver deghosting. As expected, the deghosting solution successfully removed the notches from the spectrum that are associated with the receiver ghost. In the bottom right panel in Figure 11, note the gradual recovery of the shape of the wavelet: first by receiver deghosting (middle trace) and then by source and receiver deghosting (right trace).

DISCUSSION

In deep water, the particular form of Green's theorem-derived algorithm that was applied works as well as a conventional $P + V_z$ sum. It does so without the need for a Hankel transform from coordinate space to wavenumber domain, thus avoiding the difficulty of sufficient sampling needed to support the inverse Hankel transform (Amundsen [1993], p. 1336). There are two categories of advantages in using Green's theorem: (1) avoiding demands of transforms when the measurement is on a horizontal surface, and (2) when the acquisition is not confined to a horizontal measurement surface, which precludes the use of transforms. Evaluating the advantages of the Green's theorem-derived algorithm requires side by side testing of the two algorithms as the water becomes shallower, the water bottom becomes less flat, and full 3D acquisition is used.

CONCLUSIONS

The message for the prospector or seismic processor seeking the bottom line and user-guide for seeking to source and receiver deghost marine towed streamer and ocean bottom data is as follows: (1) away from notches, a single streamer of pressure data, and an estimate of the source signature can achieve receiver deghosting, and a set of single shot records can then achieve source deghosting, and (2) if deghosting is requiring for a frequency range that includes the notches (as can occur for high-frequency towed streamer acquisition and will occur with ocean-bottom data), then we advocate measurements of the pressure and its normal derivative along a cable for receiver deghosting and a set of dual over-under source experiments to achieve source deghosting. We have implemented and tested Green's theorem-derived source and receiver deghosting for the first time on deep-water Gulf of Mexico synthetic (SEAM)

and field data. These tests indicate that the algorithm works with positive and encouraging results. The Green's theorem derived deghosting algorithms provide a unique and comprehensive framework and methodology for understanding and addressing each of these cases.

ACKNOWLEDGMENTS

We are grateful to the M-OSRP sponsors for their support of this research and the three anonymous reviewers for their constructive comments, which enhanced the clarity of this paper. The first author is also grateful to ExxonMobil and PGS for internships and Nizar Chemingui (PGS), Paolo Terenghi (M-OSRP now PGS), and the second author for mentoring.

APPENDIX A

RECEIVER DEGHOSTING: SUPPLEMENTAL THEORY

Following Weglein et al. (2002) and Chapter 2 of Zhang (2007), to separate upward-moving and downward-moving waves, we define the following (see Figure 2):

1) a reference medium consisting of a whole-space of water with wavespeed c_0,
2) a perturbation $\alpha_{\text{air}}(\mathbf{r})$ that is the difference between the reference medium (water) and the upper part (air) of the actual medium, defined by $1/c^2_{\text{air}} = 1/c^2_{\text{water}}(1-\alpha_{\text{air}})$,
3) a perturbation $\alpha_{\text{earth}}(\mathbf{r})$ that is the difference between the reference medium (water) and the lower part (earth) of the actual medium, defined by $1/c^2_{\text{earth}} = 1/c^2_{\text{water}}(1-\alpha_{\text{earth}})$,
4) V is a volume bounded above by an upper hemisphere and below by the measurement surface,
5) a surface (air-water interface) above the measurement surface (i.e., inside V),
6) a source at $\mathbf{r}_s$ above the measurement surface (again inside V),
7) a causal whole-space Green's function $G_0^+(\mathbf{r},\mathbf{r}'_g,\omega)$ in the reference medium,
8) $k_0 = \omega/c_0$,
9) the prediction/observation point $\mathbf{r}'_g \in V$ lying below the source $\mathbf{r}_s$ and above the measurement surface, and
10) S as the hemisphere's surface.

For two wavefields P and G_0^+, Green's theorem becomes

$$\oint_S \mathrm{d}S\,\mathbf{n}\cdot[P(\mathbf{r},\mathbf{r}_s,\omega)\nabla G_0^+(\mathbf{r},\mathbf{r}'_g,\omega) - G_0^+(\mathbf{r},\mathbf{r}'_g,\omega)\nabla P(\mathbf{r},\mathbf{r}_s,\omega)] = \int_V \mathrm{d}\mathbf{r}[P(\mathbf{r},\mathbf{r}_s,\omega)\nabla^2 G_0^+(\mathbf{r},\mathbf{r}'_g,\omega) - G_0^+(\mathbf{r},\mathbf{r}'_g,\omega)\nabla^2 P(\mathbf{r},\mathbf{r}_s,\omega)]. \quad \text{(A-1)}$$

Substituting the partial differential equations for the pressure wavefield P and causal whole-space Green's function G_0^+

$$(\nabla^2 + k_0^2)P(\mathbf{r},\mathbf{r}_s,\omega) = A(\omega)\delta(\mathbf{r}-\mathbf{r}_s) + k_0^2(\alpha_{\text{air}}+\alpha_{\text{earth}})P \quad \text{(A-2)}$$

$$(\nabla^2 + k_0^2)G_0^+(\mathbf{r},\mathbf{r}'_g,\omega) = \delta(\mathbf{r}-\mathbf{r}'_g) \quad \text{(A-3)}$$

into the right hand side of equation A-1 gives

$$\begin{aligned}&\int_V \mathrm{d}\mathbf{r}\{P(\mathbf{r},\mathbf{r}_s,\omega)[-k_0^2 G_0^+ + \delta(\mathbf{r}-\mathbf{r}'_g)] - G_0^+(\mathbf{r},\mathbf{r}'_g,\omega)[-k_0^2 P \\ &+ A(\omega)\delta(\mathbf{r}-\mathbf{r}_s) + k_0^2(\alpha_{\text{air}}+\alpha_{\text{earth}})P]\} \\ &= \int_V \mathrm{d}\mathbf{r}\{P(\mathbf{r},\mathbf{r}_s,\omega)\delta(\mathbf{r}-\mathbf{r}'_g) - P(\mathbf{r},\mathbf{r}_s,\omega)k_0^2 G_0^+(\mathbf{r},\mathbf{r}'_g,\omega) \\ &+ G_0^+(\mathbf{r},\mathbf{r}'_g,\omega)k_0^2 P(\mathbf{r},\mathbf{r}_s,\omega) \\ &- k_0^2[\alpha_{\text{air}}(\mathbf{r})+\alpha_{\text{earth}}(\mathbf{r})]P(\mathbf{r},\mathbf{r}_s,\omega)G_0^+(\mathbf{r},\mathbf{r}'_g,\omega) \\ &- A(\omega)\delta(\mathbf{r}-\mathbf{r}_s)G_0^+(\mathbf{r},\mathbf{r}'_g,\omega)\}. \end{aligned} \quad \text{(A-4)}$$

The first term gives $P(\mathbf{r}'_g,\mathbf{r}_s,\omega)$ because the prediction/observation point $\mathbf{r}'_g$ is between the measurement surface and air-water surface, i.e., $\in V$. The cross terms $-P(\mathbf{r},\mathbf{r}_s,\omega)k_0^2 G_0^+(\mathbf{r},\mathbf{r}'_g,\omega) + G_0^+(\mathbf{r},\mathbf{r}'_g,\omega)k_0^2 P(\mathbf{r},\mathbf{r}_s,\omega)$ cancel. (This cancellation occurs in the frequency domain but not in the time domain.) $\alpha_{\text{earth}}(\mathbf{r}) = 0$ because the volume integral doesn't contain α_{earth}. The last term gives $A(\omega)G_0^+(\mathbf{r}_s,\mathbf{r}'_g,\omega)$ because the source (air guns) is between the measurement surface and air-water surface, i.e., within the volume V. Substituting these four results into equation A-4 gives for the left member of A-4

$$P(\mathbf{r}'_g,\mathbf{r}_s,\omega) - \int_V d\mathbf{r}\,k_0^2\alpha_{air}(\mathbf{r})P(\mathbf{r},\mathbf{r}_s,\omega)G_0^+(\mathbf{r},\mathbf{r}'_g,\omega) - A(\omega)G_0^+(\mathbf{r}_s,\mathbf{r}'_g,\omega). \quad \text{(A-5)}$$

Using the symmetry of the Green's function ($G_0^+(\mathbf{r}_s,\mathbf{r}'_g,\omega) = G_0^+(\mathbf{r}'_g,\mathbf{r}_s,\omega)$) and collecting terms gives

$$\begin{aligned}&\oint_S \mathbf{n}\,\mathrm{d}S\cdot[P(\mathbf{r},\mathbf{r}_s,\omega)\nabla G_0^+(\mathbf{r},\mathbf{r}'_g,\omega) - G_0^+(\mathbf{r},\mathbf{r}'_g,\omega)\nabla P(\mathbf{r},\mathbf{r}_s,\omega)] \\ &= P(\mathbf{r}'_g,\mathbf{r}_s,\omega) - \int_V \mathrm{d}\mathbf{r}\,G_0^+(\mathbf{r},\mathbf{r}'_g,\omega)k_0^2\alpha_{air}(\mathbf{r})P(\mathbf{r},\mathbf{r}_s,\omega) \\ &- A(\omega)G_0^+(\mathbf{r}'_g,\mathbf{r}_s,\omega). \end{aligned} \quad \text{(A-6)}$$

The physical meaning of equation A-6 is that the total wavefield at $\mathbf{r}'_g$ can be separated into three parts. There are three spatially distributed sources causing the wavefield P. From the extinction theorem/Green's theorem, the left side of equation A-6 is the contribution to the field at $\mathbf{r}'_g$ due to sources outside V. There is one source outside V, $\rho_{\text{earth}} = k^2\alpha_{\text{earth}}P$. The contribution it makes at $\mathbf{r}'_g$ is $\int G_0^+\rho_{\text{earth}}$ and upgoing. The two other sources ($\rho_{\text{air}} = k^2\alpha_{\text{air}}P$ and $\rho_{\text{air guns}}$) produce a down field at $\mathbf{r}'_g$, since $\mathbf{r}'_g$ is below $\mathbf{r}_s$.

Letting the radius of the hemisphere go to ∞, the Sommerfeld radiation condition gives

$$\int_{m.s.} \mathrm{d}S\mathbf{n}\cdot[P(\mathbf{r},\mathbf{r}_s,\omega)\nabla G_0^+(\mathbf{r},\mathbf{r}'_g,\omega) - G_0^+(\mathbf{r},\mathbf{r}'_g,\omega)\nabla P(\mathbf{r},\mathbf{r}_s,\omega)] = P'_R(\mathbf{r}'_g,\mathbf{r}_s,\omega), \quad \text{(A-7)}$$

where $P(\mathbf{r},\mathbf{r}_s,\omega)$ and $\nabla P(\mathbf{r},\mathbf{r}_s,\omega)\cdot\hat{\mathbf{n}}$ are respectively the hydrophone measurements and normal derivatives (in the frequency domain), and G_0^+ is the causal whole-space Green's function for a homogeneous acoustic medium with water speed.

APPENDIX B

DERIVATION OF CONVENTIONAL $P + V_z$ SUM FROM GREEN'S THEOREM

A conventional $P + V_z$ sum receiver deghosts by decomposing P into an upgoing wavefield, P^{up}, and a downgoing wavefield, P^{down}, using

$$\left.\begin{matrix} P^{\text{up}} \\ P^{\text{down}} \end{matrix}\right\} = \frac{1}{2}(\tilde{P} \mp \frac{\rho\,\omega}{k_z}\tilde{V}_z), \tag{B-1}$$

where $\tilde{P}, \tilde{V}_z$ are plane waves and $k_z = \sqrt{(\omega/c_0)^2 - k_x^2 - k_y^2}$. Equation B-1 is equation 1 in Klüver et al. (2009), which is equation 17 in Amundsen (1993). The latter assumes a half-space of air, a water column, and a 1D layered earth.

Substituting the (acoustic) partial differential equations for the pressure wavefield $P(\mathbf{r}', \omega)$ and Green's function $G_0(\mathbf{r}, \mathbf{r}', \omega)$ into Green's second identity gives

$$\begin{aligned}\int_V d\mathbf{r}' P(\mathbf{r}', \mathbf{r}_s, \omega)\delta(\mathbf{r}' - \mathbf{r}) &= \int_V d\mathbf{r}' \rho(\mathbf{r}', \mathbf{r}_s, \omega) G_0(\mathbf{r}, \mathbf{r}', \omega) \\ &+ \oint_S dS' \hat{\mathbf{n}}' \cdot [P(\mathbf{r}', \mathbf{r}_s, \omega)\nabla' G_0(\mathbf{r}, \mathbf{r}', \omega) \\ &- G_0(\mathbf{r}, \mathbf{r}', \omega)\nabla' P(\mathbf{r}', \mathbf{r}_s, \omega)].\end{aligned} \tag{B-2}$$

See, e.g., Weglein et al. (2002) and Chapter 2 of Zhang (2007). For deghosting, use the configuration shown in Figure 2, i.e., choose

1) $\rho(\mathbf{r}', \mathbf{r}_s, \omega) = A(\omega)\delta(\mathbf{r}' - \mathbf{r}_s) + k^2[\alpha_{\text{air}}(\mathbf{r}') + \alpha_{\text{earth}}(\mathbf{r}')]P(\mathbf{r}', \mathbf{r}_s, \omega)$,
2) V is a volume bounded above by an upper hemisphere and below by the measurement surface,
3) $\mathbf{r}$ above the measurement surface and below the air/water boundary (i.e., $\in V$), and
4) G_0 a whole-space causal Green's function G_0^+.

We can start with Appendix A, equation A-7

$$\begin{aligned}P_R'(\mathbf{r}, \mathbf{r}_s, \omega) = \int_{m.s.} dS' \hat{\mathbf{n}}' \cdot [&P(\mathbf{r}', \mathbf{r}_s, \omega)\nabla' G_0^+(\mathbf{r}, \mathbf{r}', \omega) \\ &- G_0^+(\mathbf{r}, \mathbf{r}', \omega)\nabla' P(\mathbf{r}', \mathbf{r}_s, \omega)].\end{aligned} \tag{B-3}$$

For simplicity assume 2D, and equation B-3 becomes

$$\begin{aligned}P_R'(x, z, x_s, z_s, \omega) = &\int_{m.s.} dx' \\ &\times \left[P(x', z', x_s, z_s, \omega)\frac{\partial G_0^+}{\partial z'}(x, z, x', z', \omega)\right. \\ &\left. - G_0^+(x, z, x', z', \omega)\frac{\partial P}{\partial z'}(x', z', x_s, z_s, \omega)\right].\end{aligned} \tag{B-4}$$

Fourier transform equation B-4 with respect to x,

$$\begin{aligned}\int dx\, \exp(ik_x x) P_R'(x, z, x_s, z_s, \omega) = &\int dx\, \exp(ik_x x) \\ &\times \int_{m.s.} dx' \left[P(x', z', x_s, z_s, \omega)\frac{\partial G_0^+}{\partial z'}(x, z, x', z', \omega)\right. \\ &\left. - G_0^+(x, z, x', z', \omega)\frac{\partial P}{\partial z'}(x', z', x_s, z_s, \omega)\right].\end{aligned} \tag{B-5}$$

The left side of equation B-5 becomes $\tilde{P}_R'(k_x, z, x_s, z_s, \omega)$. Substitute the bilinear form of the Green's function into the right hand side of equation B-5,

$$\begin{aligned}&\int dx\, \exp(ik_x x) \\ &\times \int_{m.s.} dx' \left\{ P(x', z', x_s, z_s, \omega)\frac{\partial}{\partial z'}\right. \\ &\times \left[\frac{1}{2\pi}\int dk_x' \frac{\exp(-ik_x'(x - x'))\exp(ik_z'(z' - z))}{2ik_z'}\right] \\ &- \frac{1}{2\pi}\int dk_x' \frac{\exp(-ik_x'(x - x'))\exp(ik_z'(z' - z))}{2ik_z'}\frac{\partial P}{\partial z'} \\ &\left.\times (x', z', x_s, z_s, \omega)\right\},\end{aligned} \tag{B-6}$$

where $k_z' = \sqrt{(\omega/c_0)^2 - k_x'^2}$. Substitute $\mu = \mathbf{r} - \mathbf{r}'$ in equation B-6,

$$\begin{aligned}&\int_{m.s.} dx' \int d\mu_x\, \exp[ik_x(\mu_x + x')]\left[P(x', z', x_s, z_s, \omega)\right. \\ &\times \frac{1}{2\pi}\int dk_x' \frac{\exp(-ik_x'\mu_x)\exp(-ik_z'\mu_z)}{2ik_z'}(-ik_z')(-1) \\ &\left. - \frac{1}{2\pi}\int dk_x' \frac{\exp(-ik_x'\mu_x)\exp(-ik_z'\mu_z)}{2ik_z'}\frac{\partial P}{\partial z'}(x', z', x_s, z_s, \omega)\right] \\ &= \frac{1}{2\pi}\int_{m.s.} dx' \int d\mu_x \exp[ik_x(\mu_x + x')]\left[P(x', z', x_s, z_s, \omega)\right. \\ &\times \int dk_x' \exp(-ik_x'\mu_x) ik_z' \\ &\left. - \int dk_x' \exp(-ik_x'\mu_x)\frac{\partial P}{\partial z'}(x', z', x_s, z_s, \omega)\right]\frac{\exp(-ik_z'\mu_z)}{2ik_z'} \\ &= \frac{1}{2\pi}\int dk_x' \frac{\exp(-ik_z'\mu_z)}{2ik_z'}\int d\mu_x\, \exp(-i(k_x' - k_x)\mu_x) \\ &\times \left[ik_z'\int_{m.s.} dx'\, \exp(ik_x x')P(x', z', x_s, z_s, \omega)\right. \\ &\left. - \int dx' \exp(ik_x x')\frac{\partial P}{\partial z'}(x', z', x_s, z_s, \omega)\right].\end{aligned} \tag{B-7}$$

In equation B-7, the integral over $d\mu_x$ gives a Dirac delta, $2\pi\delta(k_x' - k_x)$, the integral over dx' is a Fourier transform of the pressure wavefield and gives $\tilde{P}(k_x, z', x_s, z_s, \omega)$, and the vertical derivative of the pressure wavefield is $i\omega\rho\, V_z(x', z', x_s, z_s, \omega)$. (The latter relationship is derived in Appendix D.) The integral of dx' over the measurement surface allows a Fourier transform because, in the derivation of equation B-3, we took the radius of the hemisphere to infinity. We now have (for the right side of equation B-5),

$$\begin{aligned}&\frac{1}{2\pi}\int dk_x' \frac{\exp(-ik_z'\mu_z)}{2ik_z'}2\pi\delta(k_x' - k_x)\left[ik_z'\tilde{P}(k_x, z', x_s, z_s, \omega)\right. \\ &\left. - i\omega\rho\int dx' \exp(ik_x x')V_z(x', z', x_s, z_s, \omega)\right].\end{aligned} \tag{B-8}$$

In equation B-8, the integral over dx' is a Fourier transform of the vertical velocity field and gives $\tilde{V}_z(k_x, z', x_s, z_s, \omega)$. Using $k_z'^2 = \omega^2/c_0^2 - k_x'^2$ and $k_z^2 = \omega^2/c_0^2 - k_x^2$, equation B-8 can be rewritten as

$$\int dk_x' \,\delta(k_x' - k_x)\frac{\exp(-ik_z'\mu_z)}{2ik_z'}[ik_z'\tilde{P}(k_x, z', x_s, z_s, \omega) - i\omega\rho\,\tilde{V}_z(k_x, z', x_s, z_s, \omega)]$$
$$= \frac{\exp(-ik_z'\mu_z)}{2ik_z'}[ik_z'\tilde{P}(k_x, z', x_s, z_s, \omega) - i\omega\rho\,\tilde{V}_z(k_x, z', x_s, z_s, \omega)]. \quad \text{(B-9)}$$

Collecting terms gives

$$\tilde{P}_R'(k_x, z, x_s, z_s, \omega) = \frac{\exp(-ik_z'\mu_z)}{2ik_z'}(ik_z) \times \left[\tilde{P}(k_x, z', x_s, z_s, \omega) - \frac{\omega\rho}{k_z}\tilde{V}_z(k_x, z', x_s, z_s, \omega)\right]$$
$$= -\frac{1}{2}\exp[ik_z'(z' - z)]\left[\tilde{P}(k_x, z', x_s, z_s, \omega) - \frac{\omega\rho}{k_z}\tilde{V}_z(k_x, z', x_s, z_s, \omega)\right]. \quad \text{(B-10)}$$

In the last equation, the phase factor $\exp(ik_z'(z' - z))$ takes the one-way wavefield $\tilde{P}_R'$ from the cable depth z' to the predicted (deghosted) depth z. This demonstrates that the Green's theorem deghosting reduces to the Fourier form equation B-10 under conditions which allow the steps in this demonstration. The standard practice deghosting $P - V_z$ algorithm today is a version of B-10 that accommodates a 3D point source, but assumes the earth is 1D. Equations B-3 and B-10 allow the lifting of the 1D assumption, and in addition B-3 doesn't require a horizontal measurement surface.

APPENDIX C

INPUT DATA

Table C-1. Synthetic data: Flat-layer-model data created using Cagniard-de Hoop code.

Parameter	Value
Number of shots	1
Number of channels per shot	1601
Number of samples per trace	625
Time sampling	4 ms
Record length	2.5 s
Shot interval	n.a.
Group interval	3 m
Shortest offset	0 m
Gun depth	7 m
Streamer depth	9 and 11 m

Air/water boundary, water depth 300 m, 1D constant velocity acoustic earth ($c = 2250$ m/s)
$\partial P/\partial z \simeq (P(11\text{ m}) - P(9\text{ m}))/2$ m
This data was created by Jinlong Yang using code written by Jingfeng Zhang (now at BP).

Table C-2. Synthetic data: SEAM deep-water Gulf of Mexico model.

Parameter	Value
Number of shots	9×267
Number of channels per shot	661×661
Number of samples per trace	2001
Time sampling	8 ms
Record length	16 s
Shot interval	150 m
Group interval	30 m
Shortest offset	0 m
Gun depth	15 m
Streamer depth	15 and 17 m

Air/water boundary, variable water depth, 3D variable density acoustic earth
3D source, frequency of source: 1–30 Hz
Distance between towed streamers: 30 m
$\partial P/\partial z \simeq (P(17\text{ m}) - P(15\text{ m}))/2$ m
Reviewer 2 pointed out that "The numerical approximation of the vertical derivative using a finite difference approach is subject to considerable error when a distance $dz = 2$ m is used. In other words, the pressure data have a much higher accuracy than the pressure derivative data when computed this way."

Table C-3. Field data: Deep-water Gulf of Mexico.

Parameter	Value
Number of shots	2451
Number of channels per shot	960
Number of samples per trace	3585
Time sampling	4 ms
Record length	14.34 s
Shot interval	32 m
Group interval	12.5 m
Shortest offset	112 m
Gun depth	9 m
Streamer depth	25 m

Data courtesy of PGS
Dual-sensor towed streamer
$\partial P/\partial z = i\omega\rho V_z$, where ρ is the density of the reference medium (seawater)

APPENDIX D

QUICK DERIVATION OF $\partial P/\partial z = i\omega\rho V_z$

1) Newton's second law of motion: $\mathbf{F} = m d\mathbf{V}/dt$
2) Consider a unit volume in a fluid: $\mathbf{F} = \rho\, d\mathbf{V}/dt$
3) Fourier transform: $\mathbf{F} = \rho(-i\omega\mathbf{V})$
4) Force in a fluid is the pressure gradient: $\mathbf{F} = -\nabla P = \rho(-i\omega\mathbf{V})$
5) Rewriting: $\nabla P = i\omega\rho\,\mathbf{V}$
6) The z-component is the desired result.

REFERENCES

Amundsen, L., 1993, Wavenumber-based filtering of marine point-source data: Geophysics, **58**, 1335–1348, doi: 10.1190/1.1443516.

Clayton, R. W., and R. H. Stolt, 1981, A Born-WKBJ inversion method for acoustic reflection data: Geophysics, **46**, 1559–1567, doi: 10.1190/1.1441162.

Corrigan, D., A. B. Weglein, and D. D. Thompson, 1991, Method and apparatus for seismic survey including using vertical gradient estimation to separate downgoing seismic wavefields: U. S. Patent number 5,051,961.

Klüver, T., P. Aaron, D. Carlson, A. Day, and R. van Borselen, 2009, A robust strategy for processing 3D dual-sensor towed streamer data: 79th Annual International Meeting, SEG, Expanded Abstracts, 3088–3092.

Kragh, E., J. O. A. Robertsson, R. Laws, L. Amundsen, T. Røsten, T. Davies, K. Zerouk, and A. Strudley, 2004, Rough sea deghosting using wave heights derived from low frequency pressure recordings — A case study: 66th Annual International Conference and Exhibition, EAGE.

Mayhan, J. D., P. Terenghi, A. B. Weglein, and N. Chemingui, 2011, Green's theorem derived methods for preprocessing seismic data when the pressure P and its normal derivative are measured: 81st Annual International Meeting, SEG, Expanded Abstracts, 2722–2726.

Mayhan, J. D., A. B. Weglein, and P. Terenghi, 2012, First application of Green's theorem derived source and receiver deghosting on deep water Gulf of Mexico synthetic (SEAM) and field data: 82nd Annual International Meeting, SEG, Expanded Abstracts, doi: 10.1190/segam2012-0855.1.

Morse, P. M., and H. Feshbach, 1953, Methods of theoretical physics: McGraw-Hill Book Co.

Osen, A., B. G. Secrest, L. Amundsen, and A. Reitan, 1998, Wavelet estimation from marine pressure measurements: Geophysics, **63**, 2108–2119, doi: 10.1190/1.1444504.

Robertsson, J. O. A., and E. Kragh, 2002, Rough-sea deghosting using a single streamer and a pressure gradient approximation: Geophysics, **67**, 2005–2011, doi: 10.1190/1.1527100.

Robinson, E. A., and S. Treitel, 2008, Digital imaging and deconvolution: The ABCs of seismic exploration and processing: SEG.

Schneider, W. A., 1978, Integral formulation for migration in two and three dimensions: Geophysics, **43**, 49–76, doi: 10.1190/1.1440828.

SEG Advanced Modeling Corporation (SEAM), 2011, The SEG advanced model: Technical report, SEG, (http://www.seg.org/resources/research/seam).

Stolt, R. H., and A. B. Weglein, 2012, Seismic imaging and inversion, **1**, Cambridge University Press.

Tan, T. H., 1999, Wavelet spectrum estimation: Geophysics, **64**, 1836–1846, doi: 10.1190/1.1444689.

Weglein, A. B., and L. Amundsen, 2003, Short note: G_0^{D0} and G_0^d integral equations relationships; the triangle relation is intact: M-OSRP 2002 Annual Report, 32–35.

Weglein, A. B., F. V. Araújo, P. M. Carvalho, R. H. Stolt, K. H. Matson, R. T. Coates, D. Corrigan, D. J. Foster, S. A. Shaw, and H. Zhang, 2003, Inverse scattering series and seismic exploration: Inverse Problems, **19**, R27–R83, doi: 10.1088/0266-5611/19/6/R01.

Weglein, A. B., and B. G. Secrest, 1990, Wavelet estimation for a multidimensional acoustic earth model: Geophysics, **55**, 902–913, doi: 10.1190/1.1442905.

Weglein, A. B., S. A. Shaw, K. H. Matson, J. L. Sheiman, R. H. Stolt, T. H. Tan, A. Osen, G. P. Correa, K. A. Innanen, Z. Guo, and J. Zhang, 2002, New approaches to deghosting towed-streamer and ocean-bottom pressure measurements: 72nd Annual International Meeting, SEG, Expanded Abstracts, 1016–1019.

Weglein, A. B., R. H. Stolt, and J. D. Mayhan, 2011a, Reverse-time migration and Green's theorem: Part I — The evolution of concepts, and setting the stage for the new RTM method: Journal of Seismic Exploration, **20**, 73–90.

Weglein, A. B., R. H. Stolt, and J. D. Mayhan, 2011b, Reverse time migration and Green's theorem: Part II — A new and consistent theory that progresses and corrects current RTM concepts and methods: Journal of Seismic Exploration, **20**, 135–159.

Zhang, J., 2007, Wave theory based data preparation for inverse scattering multiple removal, depth imaging and parameter estimation: Analysis and numerical tests of Green's theorem deghosting theory: Ph.D. thesis, University of Houston.

Zhang, J., and A. B. Weglein, 2005, Extinction theorem deghosting method using towed streamer pressure data: analysis of the receiver array effect on deghosting and subsequent free surface multiple removal: 75th Annual International Meeting, SEG, Expanded Abstracts, 2095–2098.

Zhang, J., and A. B. Weglein, 2006, Application of extinction theorem deghosting method on ocean bottom data: 76th Annual International Meeting, SEG, Expanded Abstracts, 2674–2678.